Plasma Chem Plasma Process (2017) 37:805–823
DOI 10.1007/s11090-017-9809-7

ORIGINAL PAPER

A Coupled Chemical Kinetic and Nucleation Model of Fume Formation in Metal–Inert-Gas/Metal–Active-Gas Welding

Hunkwan Park[1] · Maximilian Mudra[1,2] · Marcus Trautmann[1,3] · Anthony B. Murphy[1]

Received: 14 December 2016 / Accepted: 1 March 2017 / Published online: 13 March 2017

Abstract A computational model of the formation of welding fume in arc plasmas, under conditions occurring in metal–inert-gas (MIG) and metal–active-gas (MAG) welding, is presented. The model couples the chemical kinetics occurring in high-temperature mixtures of iron vapour, oxygen and argon with a moment model of the nucleation and growth by condensation of iron and iron oxide nanoparticles. Results are presented for different iron vapour concentrations, oxygen-to-argon ratios, and quench rates. It is found that the presence of oxygen has important effects on the gas-phase chemistry and the properties of the nanoparticles. FeO nanoparticles are preferentially nucleated, and have smaller diameter than the Fe nanoparticles that are produced in the absence of oxygen. The final composition of the nanoparticles depends on the relative concentrations of iron and oxygen in the plasma. A three-dimensional arc model that includes vaporization of the wire electrode is used to predict temperature, velocity and iron vapour mass fraction distributions in typical MIG and MAG welding conditions. Calculations of nanoparticle formation and growth along streamlines confirm the importance of oxygen in determining the fume particle properties.

Keywords Welding fume · Gas metal arc welding · MIG welding · MAG welding · Nanoparticle formation · Nucleation · Condensation · Computational modelling

✉ Anthony B. Murphy
tony.murphy@csiro.au

[1] CSIRO Manufacturing, PO Box 218, Lindfield, NSW 2070, Australia

[2] University of the Federal Armed Forces Munich, Werner Heisenberg Weg 39, 85577 Neubiberg, Germany

[3] Institute of Manufacturing Technology, Dresden University of Technology, George-Bahr-Str. 3c, 01069 Dresden, Germany

Introduction

Welding fume is an unavoidable by-product of the vaporization of molten metal that occurs in arc welding. Fume is mainly produced by nucleation of the metal vapour to form nanoparticles; these nanoparticles subsequently grow through condensation of additional vapour, and coagulation to form larger particles or chains of smaller particles.

Welding fume is a significant occupational health problem, which particularly affects the respiratory and cardiovascular systems [1–3]. Both the dimensions and composition of the fume particles can cause problems. The typical sizes of the chains of particles are such that they can become lodged in regions of the lungs from which they are not easily cleared. Further, chromium, nickel and manganese, which are present in fume when stainless steel is welded, have carcinogenic or neurotoxic properties.

The most widely-used form of arc welding in manufacturing industry is MIG/MAG welding (metal–inert-gas/metal–active-gas welding, also known as GMAW or gas–metal arc welding). In MIG welding, an inert gas, usually argon, is used as the shielding gas. In MAG welding, oxygen or carbon dioxide is added to the argon; pure carbon dioxide can also be used. When welding iron or steel, the fume particles are composed mainly of iron oxide. In MIG welding, the initial nanoparticles can be composed of iron if the shielding is thorough, since there is no oxygen in the shielding gas; oxidation will then occur subsequently at the edge of the arc. In MAG welding, oxygen is present in the arc, so it is possible that the initial nanoparticles are composed of iron oxide.

Several approaches have applied to modelling of nanoparticle formation and growth in thermal plasmas [4], of which welding arcs are an example. Those relevant to iron nanoparticle production include the discrete–sectional model of Girshick et al. [5], which was applied to conditions of an atmospheric-pressure radio-frequency inductively-coupled plasma (RF ICP), with iron vapour mole fraction of order 1% and quench rates slower than 10^5 K s^{-1}. Subsequently, Girshick et al. [6, 7] extended their model to include coagulation, and developed a moment model coupled to a two-dimensional model of an RF ICP reactor; Bilodeau and Proulx [8] used a similar approach to model iron nanoparticle production in an RF ICP reactor. Several experimental papers on synthesis of iron and iron oxide particles have been published, including [9] and the references provided therein.

Models of fume formation in welding arcs have been, in contrast to the above models of iron nanoparticle formation, relatively unsophisticated until fairly recently, using semi-empirical approaches to estimate the total amount of fume formed and the location of the formation process (e.g., [10]). Recently, however, the work of Tashiro et al. [11, 12], Boselli et al. [13] and Sanibondi [14] has used more rigorous physics-based approaches.

Most computational models of fume formation neglect the presence of oxygen in the arc, instead assuming that the fume is formed of iron nanoparticles. Tashiro et al. [15] used a one-dimensional model of nucleation and condensation of iron nanoparticles, and a two-dimensional model of coagulation, to predict the size and shape of fume particles, including particle chains, formed in MIG welding. Subsequently, Tashiro et al. [12] improved their coagulation model by including the influence of particle charging and Brownian motion on the particle motion, and by allowing the particle temperature to differ from the gas temperature. In both cases, the time-dependence of temperature and the initial partial pressure of metal vapour were derived from two-dimensional models of arc welding. Boselli et al. [13] coupled a two-dimensional model of MIG welding to a moment model of fume formation that takes into account nucleation, condensation and coagulation. The coupled model allowed the prediction of the distribution of the fume production in the

region surrounding the arc, although the shape of the particles could not be calculated. Vishnyakov et al. [16] used an approach derived from modelling of dusty plasmas to examine the influence of ion-induced nucleation on nucleation and condensation of iron vapour in shielded metal arc welding, extending this to include coalescence of the particles [17] and condensation of the components other than iron vapour that are derived from vaporization of the coated wire electrode used in this type of welding [18].

Only the recent paper of Sanibondi [14] has considered the influence of oxygen in fume formation. He considered nucleation of Fe and FeO nanoparticles, and their growth by condensation and coagulation, as well as oxidation reactions between gas-phase species and nanoparticles. The calculation was one-dimensional, using the time-dependence of temperature and initial partial pressure of metal vapour taken from the MIG welding model of Tashiro et al. [15]. The initial composition of the gas before nucleation was obtained assuming chemical equilibrium, with assumed oxygen partial pressures added to the argon–iron-vapour mixture obtained from the MIG welding model.

In our work, we present a chemical kinetic model that includes the important gas-phase species, and couple this to a model of nucleation and condensation; this allows both the composition and mean size of the nanoparticles to be predicted. We further combine the model with temperature and compositions along streamlines obtained from a three-dimensional model of the MIG/MAG welding arc. Our work therefore has two advantages over that of Sanibondi; we do not assume chemical equilibrium for the initial gas composition, and we use time-dependence of temperature and metal-vapour partial pressure obtained from a welding model in which oxygen is included. However, unlike Sanibondi, we do not consider coagulation or oxidation of the solid particles, and our model is only able to predict the average particle size, not the distribution of sizes.

We first present the methods we use in the chemical kinetics, particle formation and welding arc models. We next present a series of results for constant quench rates to establish the dependence of particle properties on the iron vapour and oxygen concentrations and the quench rate. We then investigate the formation of fume particles in a MIG arc in pure argon, and MAG arcs with oxygen added to the argon.

Methods

Chemical Kinetics

We consider the following gas-phase species in the model: Fe, FeO, FeO_2, O_2, O and Ar. Since nucleation of nanoparticles occurs at temperatures below the boiling temperature of the material of which they are composed, it is reasonable to neglect the presence of ionized species, which are not present in significant amounts until the temperature reaches well above the boiling temperatures.

The following chemical reactions were considered:

$$\begin{aligned} &O + Fe + M \leftrightarrow FeO + M \\ &Fe + O_2 \leftrightarrow FeO + O \\ &Fe + O_2 + M \leftrightarrow FeO_2 + M \\ &FeO + O + M \leftrightarrow FeO_2 + M \\ &FeO_2 + O \leftrightarrow FeO + O_2 \\ &O_2 + M \leftrightarrow O + O + M \end{aligned} \tag{1}$$

where M represents any third species. The forward reaction rates were taken from [19]. The reverse reaction rates were determined from the equilibrium constant, with the Gibbs free energy taken from the JANAF tables [20].

Nucleation and Condensation

We use the kinetic nucleation rate recommended by Girshick and Chiu [21] to calculate the nucleation rate of a species i:

$$J_i = v_i \left(\frac{2\sigma_i}{\pi m_i}\right)^{1/2} n_{si}^2 S_i \exp\left[\Theta_i - \frac{4\Theta_i^3}{27(\ln S_i)^2}\right] \tag{2}$$

where σ_i is the surface tension, $n_{s\,i}$ is the saturation number density, $S_i = n_i/n_{s\,i}$ is the supersaturation and $\Theta_i = \sigma_i s_i/kT$ is the dimensionless surface energy of species i; k is Boltzmann's constant, T is the temperature, and v_i, m_i, n_i and s_i are respectively the volume, mass, number density and surface area of a monomer of species i. It is assumed that clusters are stable once they reach the critical particle size

$$d_i^* = \frac{4\sigma_i v_i}{kT \ln S_i} \tag{3}$$

The rates of change of the total number density of particles N, total diameter of particles per unit volume M and total surface area of particles per unit volume A are calculated using the moment model derived by Friedlander [22], adapted to treat multiple species:

$$\frac{dN}{dt} = \sum_i J_i \tag{4}$$

$$\frac{dM}{dt} = \sum_i \left[J_i d_i^* + (S_i - 1) b_i N\right] \tag{5}$$

$$\frac{dA}{dt} = \sum_i \left[J_i k_i^{*2/3} s_i + 2\pi b_i (S_i - 1) M\right] \tag{6}$$

where k_i^* is the number of monomers in a particle of critical size and $b_i = 2n_{s\,i} v_i \sqrt{kT/2\pi m_i}$. The first term on the right-hand sides of Eqs. (4)–(6) describes the influence of nucleation, and the second term on the right-hand sides of Eqs. (5) and (6) describes condensation.

The rate of change of the number density of a gas phase species i is given by

$$\frac{dn_i}{dt} = R_i - J_i k_i^* - (S_i - 1)\frac{b_i A}{2v_i} \tag{7}$$

where R_i is the net rate of production of the species by gas-phase chemical reactions, calculated using standard chemical kinetics approaches, and the second and third terms on the right-hand side describe the loss of the species by nucleation and condensation, respectively. There are three species for which nucleation and condensation are possible: Fe, FeO and FeO_2. For the other three species (Ar, O and O_2), only the first term on the right-hand side of Eq. (7) is used. In practice, the concentration of FeO_2 is found to be so low that its nucleation does not occur.

Physical Data for Condensed Species

The surface tension was assumed to follow a linear dependence:

$$\sigma = \sigma_0 + (T - T_0)\left.\frac{d\sigma}{dt}\right|_{T_0} \tag{8}$$

Data for surface tension of both species were taken from Sanibondi [14], and are presented in Table 1. The saturation number densities were calculated from the boiling temperature and latent heat of vaporization using the ideal gas law

$$n_{s\,i} = P_{\mathrm{vap}\,i}/kT \tag{9}$$

and the vapour pressure of species i, obtained using the Clausius–Clapeyron equation:

$$P_{\mathrm{vap}\,i} = P_{\mathrm{atm}} \exp\left[\frac{-H_{\mathrm{vap}\,i}}{R}\left(\frac{1}{T} - \frac{1}{T_{b\,i}}\right)\right] \tag{10}$$

where P_{atm} is atmospheric pressure, $H_{\mathrm{vap}\,i}$ is the molar heat of vaporization of species i, $T_{b\,i}$ is the boiling temperature of species i at atmospheric pressure, and R is the ideal gas constant. Values of $T_{b\ i}$ and $H_{\mathrm{vap}\ i}$, from [20] and [23], are given in Table 1.

Coupled Chemical Kinetic and Particle Growth Model

The set of coupled partial different equations used to determine the gas-phase composition and the particle number density and size (Eqs. (4)–(6), and Eq. (7) for each species) defines an initial-value problem. This was solved using the Radau IIA method of order 5, 9 and 13 [24, 25], which is a type of Runge–Kutta method. The code for the execution, step-size adaption and variable order was taken from [25].

As gas-phase species nucleate and condense, the number of gaseous particles decreases, which leads to a decreasing pressure. In reality, this does not occur, since the resulting pressure gradient leads to replacement of the gas-phase molecules that are removed by the surrounding gas. To address this problem, the condensed molecules are replaced by argon to maintain the pressure at 1 atm. This is more realistic than the alternative of adding argon, iron and oxygen in the ratio prior to the occurrence of nucleation for two reasons. First, the alternative approach would add additional iron and oxygen to the system. Second, nucleation and condensation will occur at approximately the same rate in adjacent regions of the arc, so there will be no iron and oxygen available to replace the condensed species.

Arc Welding Model

We use a three-dimensional model of MIG/MAG welding in which the arc, wire electrode and workpiece are included self-consistently. The model assumes local thermodynamic

Table 1 Property data for condensed species

Species	σ_0 (mN m^{-1})	$d\sigma/dT\|_{T_0}$ (mN m^{-1} K^{-1})	T_0 (K)	T_b (K)	H_{vap} (kJ mol^{-1})
Fe	2029	−0.619	1808	3134	340
FeO	585	0.63	1700	3678	402

equilibrium (LTE), and is based on that of Murphy [26] that was used to predict the production of metal vapour in MIG welding of aluminium. The main change is that an iron wire electrode and workpiece were used instead of aluminium, and it was assumed the surface of the workpiece remains flat; i.e. deformation of the workpiece due to the transfer of droplets from the wire electrode was neglected. Results were obtained for pure argon, and argon–oxygen shielding gases; it was assumed that the argon and oxygen remain fully mixed.

The vaporization of the wire electrode was calculated self-consistently, as described previously [26], and the diffusion of the iron vapour and the shielding gas was calculated using the combined diffusion coefficient method [27, 28]. Thermodynamic and transport properties of the plasma were calculated following Murphy and Arundell [29] and Murphy [30]. Net radiative emission coefficients for argon and oxygen were calculated using the method of Cram [31], and those for iron vapour from the work of Menart and Malik [32], with interpolation on a mole-fraction basis as recommended by Gleizes et al. [33].

The quench rate and iron vapour concentrations along streamlines were calculated from the temperature, flow velocity and iron vapour distributions predicted by the model. The metal vapour mole fraction from the arc model is only used until the commencement of nucleation. Once nucleation starts, the iron concentration is then calculated from the particle growth model. However, the temperature predicted by the arc model continues to determine the quench rate throughout the growth of the particles.

Results

Calculations Using Constant Quench Rate

Initial calculations were performed to determine the dependence of the particle size and number density on three important parameters: the iron vapour concentration, the oxygen-to-argon ratio and the quench rate.

Figure 1a shows the changes in the gas composition for conditions typical of the edge regions of a MAG welding arc: an iron vapour concentration of 20 mol%, a 5.26 mol% oxygen-to-argon ratio, and a quench rate of -10^7 K s^{-1}. The argon mole fraction is not shown; it was initially 0.76 and subsequently increased. At high temperatures, the main reactive species are Fe and O; as the gas cools, the FeO mole fraction increases. Very little FeO_2 is formed. The mass fractions of the reactive species falls rapidly to zero once the temperature falls below 2500 K as nucleation commences.

The supersaturation, nucleation rate and other parameters relevant to the particle formation are shown in Fig. 1b. Despite its much lower mole fraction, the supersaturation of FeO is much higher than that of Fe. This is a consequence of the much higher boiling temperature of FeO, which means that its vapour pressure is lower at a given temperature; this point is discussed in more detail below. The only species for which nucleation occurs is FeO, which initially forms particles of diameter about 2 nm. Note that for temperatures above 2650 K, the particle number density is very low, so the calculated particle diameter is not important. The particles initially grow through condensation of FeO; condensation of Fe commences when the temperature falls below 2500 K. All the Fe and FeO has condensed before the temperature reaches 2000 K. The composition of the particle is therefore determined by the initial Fe:O ratio, which is in this case 5:1.

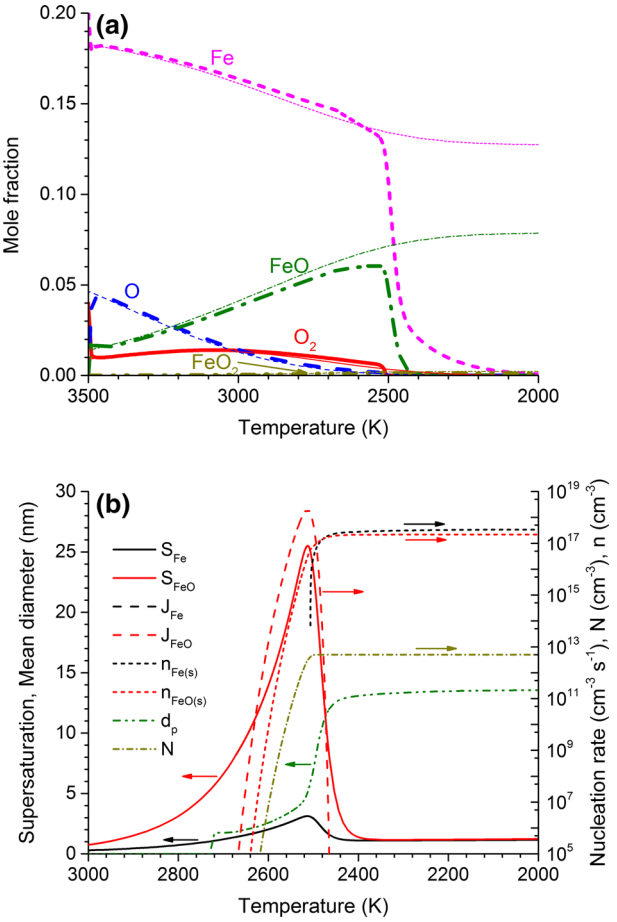

Fig. 1 Gas composition and nucleation parameters for initial gas composition of 20 mol% Fe, O_2/Ar = 5.3 mol%, and quench rate -10^7 K s^{-1}. **a** Gaseous species mole fractions; for clarity, argon is not shown; its mole fraction is initially 0.76, and increases when nucleation occurs. Results obtained using gas-phase chemical kinetics (*thick lines*) and a chemical equilibrium calculation (*thin lines*) are compared. **b** Supersaturation *S*, nucleation rate *J*, number of condensed atoms *n* of Fe and FeO; mean particle diameter d_p and particle number density *N*

The gas composition and particle parameters for a higher iron vapour concentration of 60 mol% are shown in Fig. 2a, b, respectively. In this case, because of the much higher Fe mole fraction, supersaturation of Fe is only a little lower than that of FeO. This means that nucleation of both species occurs. Nucleation of FeO becomes significant at a temperature of around 2560 K, with the initial particle diameter of about 8 nm. The particles grow by condensation of FeO, with nucleation and condensation of Fe becoming important at about 2500 K. At this point, there is a small decrease in average particle size before growth recommences. The initial Fe:O ratio is 30:1, which as before determines the particle composition.

Figures 1a and 2a also show comparisons of the gas composition calculated assuming chemical equilibrium with the composition obtained using gas-phase chemical kinetics. For an initial Fe mole fraction of 20% (Fig. 1a), the Fe and O mole fractions predicted

using the chemical kinetic model are higher, and the FeO and O_2 mol fractions lower, than obtained with the chemical equilibrium calculation; the FeO/Fe mole ratio is decreased by 10% just prior to the commencement of nucleation. This indicates that the finite rates of the recombination reactions to form FeO and O_2 have a significant influence for these conditions. For an initial Fe mole fraction of 60% (Fig. 2a), in contrast, there is no significant difference between the two calculations. Note that once nucleation commences, the chemical equilibrium calculations presented in Figs. 1a and 2a do not track the gas composition. It is possible, however, to calculate the equilibrium composition taking into account the iron and oxygen species removed by particle nucleation and growth [14]. The rapid change in gas phase composition during this process means that the chemical equilibrium composition is likely to deviate from that calculated using chemical kinetics.

These results indicate, for the quench rate considered here, gas-phase chemical kinetic calculations give a lower FeO/Fe gas-phase mole ratio than in chemical equilibrium, for low-to-moderate iron vapour concentrations. The importance of taking into account

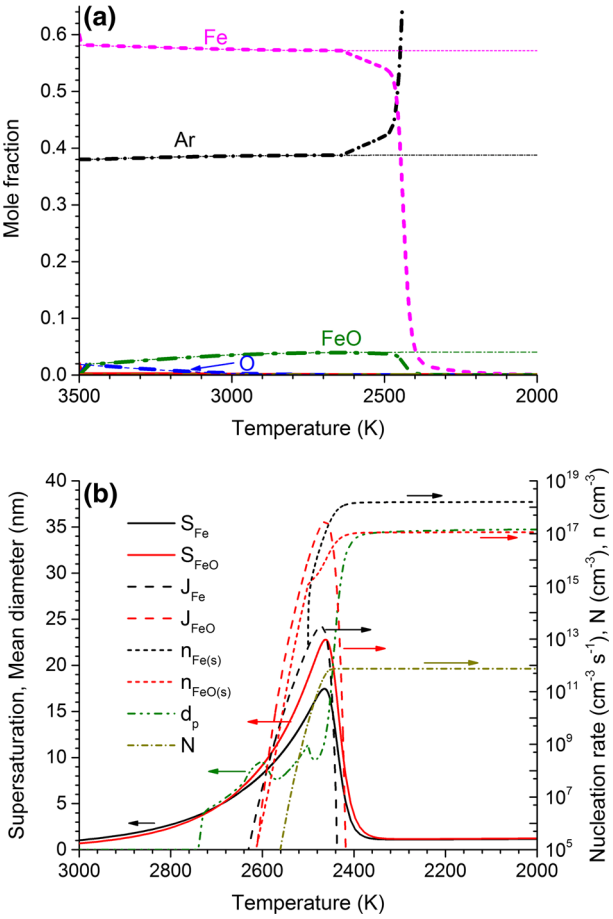

Fig. 2 As for Fig. 1, for initial gas composition of 60 mol% Fe, O_2/Ar = 5.3 mol%. Results obtained using gas-phase chemical kinetics (*thick lines*) and a chemical equilibrium calculation (*thin lines*) are compared in (**a**)

chemical kinetics will of course increase for higher quench rates. However, a complete assessment of the importance of taking into account chemical kinetics would require a direct comparison of the particle properties obtained when the gas-phase composition is calculated using chemical kinetics, as done here, and when the composition is calculated using chemical equilibrium, as was done by Sanibondi [14].

The dependence on the oxygen-to-argon ratio of the nucleation rate of Fe and FeO is shown in Fig. 3 for initial iron vapour concentrations of 20 and 60 mol%. Only a small amount of oxygen is necessary for the nucleation rate of FeO to exceed that of Fe. This is because, as noted above, the higher boiling point of FeO means it has a lower vapour pressure at a given temperature. The supersaturation is inversely proportional to the vapour pressure (or, equivalently, the saturation number density), and the nucleation rate increases rapidly with the supersaturation. Only for low oxygen-to-argon ratios is the ratio of the number densities of Fe to FeO high enough for the Fe nucleation to dominate. As the iron vapour concentration decreases, so does the threshold oxygen-to-argon ratio for which FeO nucleation begins to dominate.

The influence of the presence of oxygen on the final number density and mean diameter of particles is shown in Fig. 4. A larger number of smaller particles is generated once the oxygen content is sufficient for FeO particles to be generated; for the case shown in the figure (60 mol% Fe), this occurs for oxygen-to-argon ratios above about 2 mol%. This is because the nucleation rate of FeO is much more rapid than that of Fe, as shown in Fig. 3. The faster nucleation rate leads to a higher number of particles being produced, so fewer gas molecules are available per particle for condensation.

The iron vapour concentration also affects the final particle mean diameter, as shown in Fig. 5. As was shown in Fig. 3, lower oxygen-to-argon ratios are required for nucleation of FeO, rather than Fe, to occur when the iron vapour concentration decreases. This means that the rapid drop in particle size occurs for lower oxygen-to-argon ratios as the iron vapour concentration decreases.

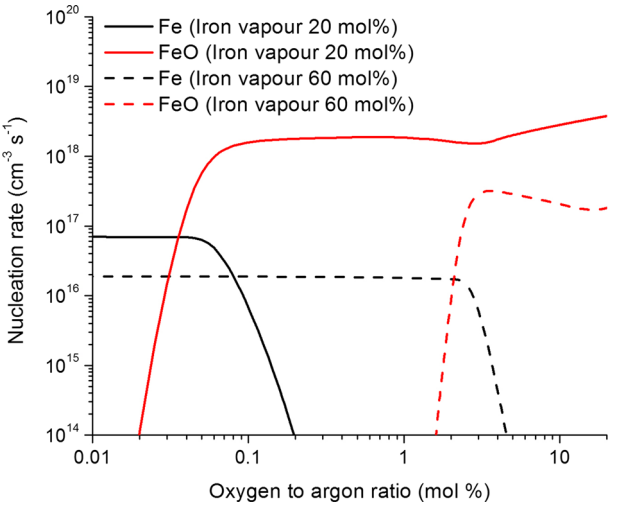

Fig. 3 Influence of the initial O_2/Ar ratio on the peak nucleation rate of Fe and FeO for 20 and 60 mol% Fe, quench rate -10^7 K s^{-1}

For lower iron vapour concentrations, the particles are smaller for all oxygen-to-argon ratios; this means they have a higher number density, since the number density varies inversely with the particle size. Low iron vapour concentration decreases the particle size through two mechanisms. First, supersaturation occurs at lower temperatures, leading to a higher nucleation rate. Second, there are fewer Fe atoms or FeO molecules available for condensation onto the particles that are formed.

Finally, we examine the influence of the quench rate on the particle formation. Figure 6 shows the dependence of the supersaturation of FeO on quench rate for the case of 60 mol% Fe and 5 mol% oxygen-to-argon ratio. As the quench rate is increased, nucleation is delayed, allowing the supersaturation to reach a higher level. The means that nucleation is more rapid when it finally occurs. As a consequence, the mean particle diameter decreases as the quench rate increases, as shown in Fig. 7. As was shown in Fig. 5, the particle diameter decreases for lower iron vapour concentrations.

Arc Calculations

The previous results were obtained using assumed initial iron vapour concentrations and quench rates, with the quench rate maintained constant throughout the particle formation and growth. In this subsection, we use iron vapour concentrations and quench rates obtained from a three-dimensional model of arc welding. Three shielding gas compositions are considered: pure argon, a mixture of argon and 1 mol% oxygen, and a mixture of argon and 5 mol% oxygen. Results are presented for an arc current of 200 A and an iron electrode of diameter 1.2 mm and fed at a rate of 100 mm s^{-1}. For simplicity, a stationary arc was modelled; this means the arc is axisymmetric for the cases considered here.

Figure 7 shows predicted iron vapour mass fraction and temperature distributions in a vertical cross-section through the arc for the three shielding gas compositions. The highest arc temperature occurs directly below the wire electrode for all cases. The inclusion of 5 mol% oxygen leads to a more constricted arc and a slightly higher maximum temperature (15,200 K compared to 14,800 K for pure argon). This increase is similar to the 3.8% increase in maximum temperature found by Jönsson et al. [34] for an arc current of 250 A, and is a consequence of the small differences in the thermophysical properties of argon and

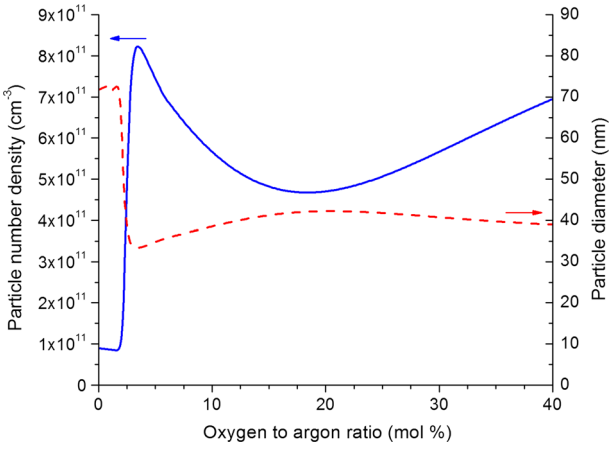

Fig. 4 Dependence on the initial O_2/Ar ratio of final particle number density and particle diameter for 60 mol% Fe, quench rate -10^7 K s^{-1}

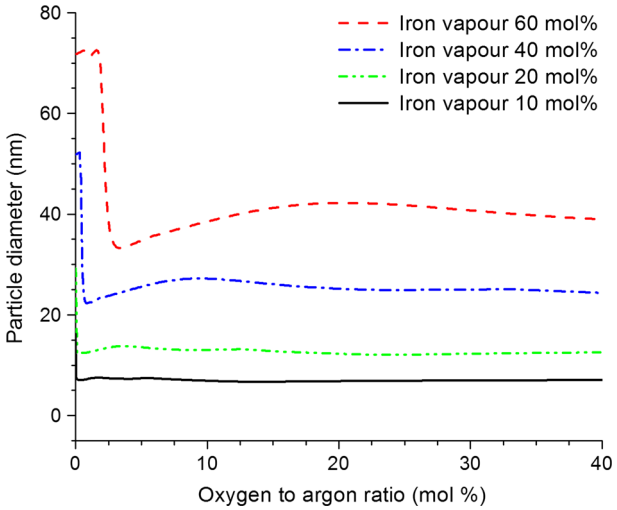

Fig. 5 Comparison of dependence of final particle mean diameter on the initial O_2/Ar ratio for different initial iron mole fractions for quench rate of -10^7 K s^{-1}

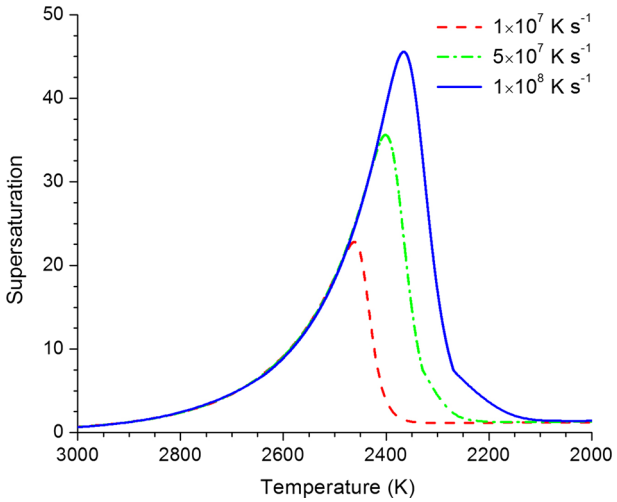

Fig. 6 Supersaturation as the temperature decreases for different quench rates with 5 mol% oxygen-to-argon ratio and 60 mol% Fe

the argon–oxygen mixture [29, 34, 35]. The vaporization rate of the tip of the wire anode is in all cases about 1% of the mass feed rate of the wire. The vaporization rate is slightly higher for the 5 mol% oxygen case (8.16 mg s^{-1}) than for pure argon (8.10 mg s^{-1}), due to a higher arc temperature near the electrode tip. The temperature near the arc axis is decreased due to the high concentration of iron vapour, leading to a local temperature minimum on axis, as found in other models of MIG/MAG arcs that include the influence of iron vapour [36–38].

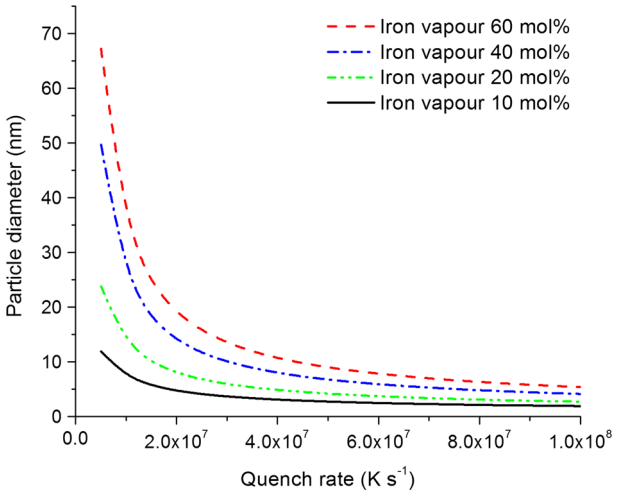

Fig. 7 Dependence of final mean particle diameter on quench rate for 5 mol% oxygen-to-argon ratio

The particle formation model was coupled to the arc model using the iron vapour mole fraction, the temperature and the flow velocity along streamlines. This provides the dependence of iron vapour mass fraction on time and the quench rate. Figure 8c show streamlines starting at the four positions, labelled A, B, C and D, which cover various quench rates and iron vapour concentrations. Particle formation does not commence until the streamlines approach the fringes of the arc, where the temperature falls below 3000 K.

Figure 9 shows the fume particle formation process for the streamline starting at position A for the 5 mol% oxygen case. Nucleation commences when the temperature falls below 2800 K. The iron vapour mole fraction at this stage is about 15 mol%, and the quench rate is -7.7×10^6 K s^{-1}. Initially, the mean particle diameter is 2 nm, which is maintained for a short time. As the temperature decreases further, nucleation becomes more rapid, and condensation soon leads to an increase in particle diameter until a final mean diameter 17 nm is reached. Similar trends are observed for pure argon and the argon with 1 mol% oxygen cases, although the mean particle diameter is significantly larger for the pure argon case.

Since values of temperature, mass fraction and velocity are obtained at discrete mesh points in the arc model, interpolation is required for their use as input data for the particle formation model. The short time scale of particle nucleation and growth, and the relative coarseness of the mesh required to obtain an acceptable convergence time in the arc model, mean that the results are somewhat dependent on the location of the nucleation with respect to the mesh points. For clarity, in comparing results for the three gas mixtures, we therefore show results averaged over the four streamlines.

The final mean particle diameter and number density, averaged over the four streamlines, are compared for the three gas mixtures in Fig. 10. We find that particles of the largest diameter and the smallest number density are formed in the case of pure argon. As was found in the previous subsection, inclusion of oxygen in shielding gas leads to a higher number density of smaller particles due to much faster nucleation of FeO. These results confirm that the presence of oxygen plays an important role in the particle formation process.

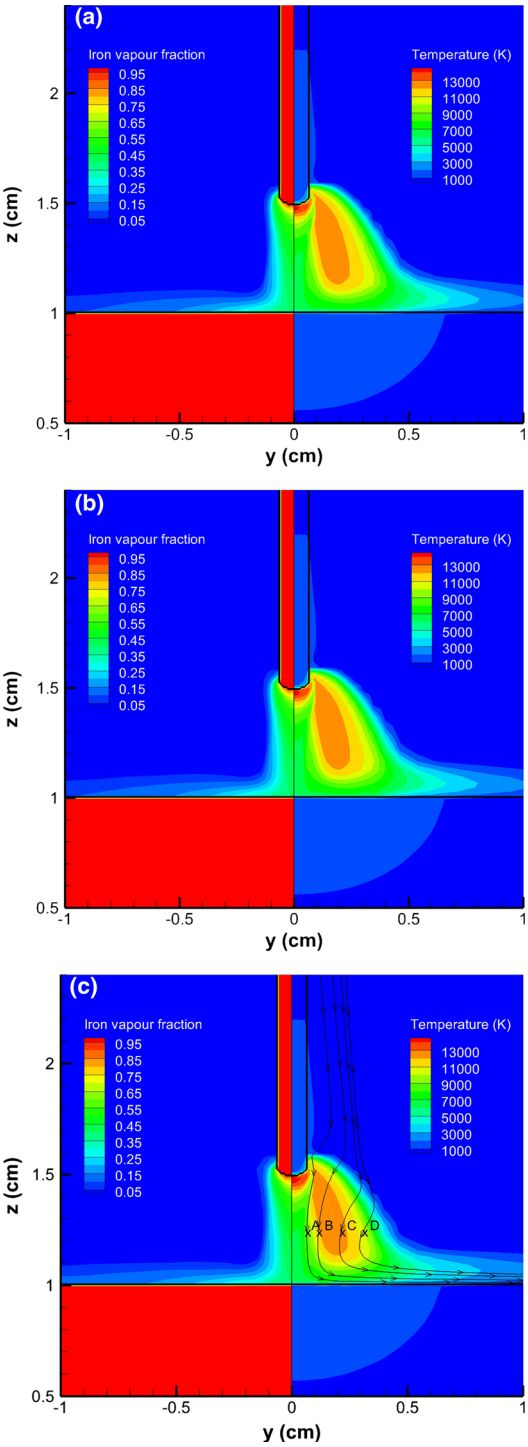

Fig. 8 Iron vapour mass fraction (*left*) and temperature (*right*) distributions in a vertical plane through the centre of the arc: **a** 100 mol% Ar, **b** Ar + 1 mol% O_2, **c** Ar + 5 mol% O_2. The maximum temperature in the three cases is 14,800, 14,900 and 15,200 K, respectively, and the wire vaporization rate is 8.10, 8.11 and 8.16 mg s^{-1}, respectively. Selected streamlines are shown with the temperature distribution of the Ar + 5 mol% O_2 arc

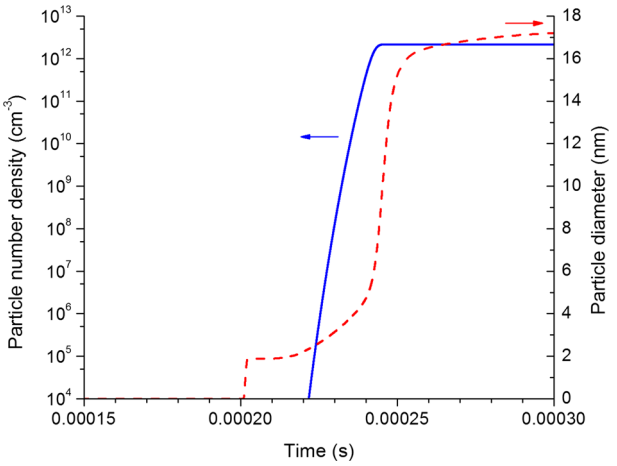

Fig. 9 Evolution of the mean particle diameter and number density along the streamline A in Fig. 8c

Figure 10 further shows that the final mean particle diameter for the 5 mol% oxygen case is slightly smaller than for the 1 mol% oxygen case. For the relatively small iron vapour mole fractions that occur in the regions where particle formation occurs (10–20%), the particle size is expected to be similar for 1 or 5% oxygen, as shown in Fig. 5. However, the quench rate for the 1 mol% oxygen case is larger than that for the 5 mol% case, which leads to the formation of a higher number density of smaller particles. In a MAG arc, it is expected that a range of particle sizes will be formed, depending on the iron vapour mass fraction and temperature distribution, as well as the oxygen-to-argon ratio, in the temperature range for which nucleation and condensation occur.

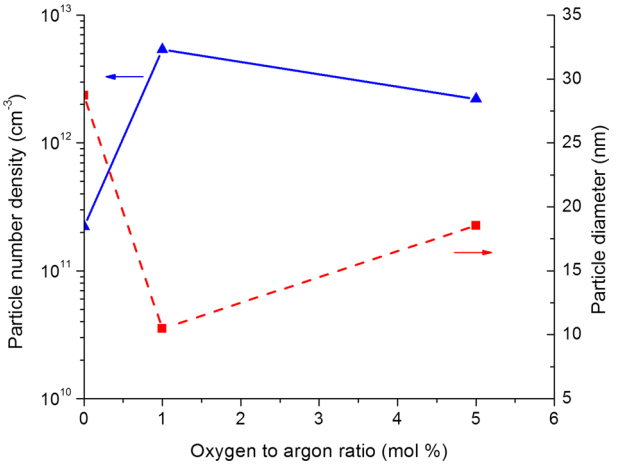

Fig. 10 Average values of the final particle diameter and number density for the selected streamlines for the three different gas mixtures considered in Fig. 8

Discussion

As noted in the introduction, the only other published model to consider the influence of oxygen on fume formation was that of Sanibondi [14]. He presented results for a quench rate of -3.5×10^5 K s^{-1}, which is lower than we have considered. For the highest iron vapour concentration he considered, 5 mol%, and an oxygen-to-argon ratio of 2 mol%, a primary particle diameter of 60 nm was predicted. Figure 7 shows that the particle size increases rapidly as the quench rate decreases, although the mean diameter for the lowest quench rate we consider, -5×10^5 K s^{-1}, is still significantly smaller than 60 nm for lower iron vapour mole fractions. Sanibondi also considered the influence of oxygen-to-argon ratio on the particle size, but only provided results for 0.7 mol% iron vapour concentration. In this case, the particle diameter decreased as the oxygen-to-argon ratio increased from 10^{-9} to 2×10^{-3} mol%, and then increased as the ratio increased further. For the lowest ratio, Sanibondi found that Fe nucleated, while for the higher ratios, only FeO nucleated. His results therefore show the same qualitative trend as ours—when the oxygen concentration is very low, only Fe nucleates, and the particle size is larger than that predicted for higher oxygen concentrations, for which FeO nucleates.

In our model, the composition of the final fume particles is determined by the iron-vapour-to-oxygen ratio at the start of the particle growth process. If there are more iron vapour atoms than oxygen atoms present, then the particles will be a mixture of Fe and FeO, since the excess iron atoms will condense on the FeO nanoparticles that are nucleated. If the iron vapour to oxygen ratio is very high, then Fe nanoparticles will also nucleate. If there is excess oxygen present, then the particles will be essentially pure FeO, since only FeO nanoparticle will nucleate, and since condensation of FeO will dominate over that of Fe.

We note that in reality, the nanoparticles that are formed will be subject to further oxidation in the presence of excess oxygen. Sanibondi [14] considered the subsequent oxidation of the Fe and FeO nanoparticles that were formed, and found that for high concentrations of oxygen, Fe_2O_3 and Fe_3O_4 particles were formed. This is in accordance with measurements of fume formation in welding arcs [14], and also experiments on iron and iron oxide nanoparticle formation in other thermal plasma systems (see [9] and references therein).

Our model allows us to predict the mean particle size of the primary nanoparticles produced during the fume formation process. The primary particles typically agglomerate to form chains or networks of particles, up to several micrometres long [15]. Prediction of the formation of such chains requires calculation of trajectories and collisions of the primary particles in a two- or three-dimensional model. Tashiro et al. [12, 15] have performed such calculations in two dimensions, finding that factors including the temperature of the particles, the Brownian motion of the particles as they interact with gas molecules, the charging of the particles, and the increased electron density in the arc fringes due to deviations from local thermodynamic equilibrium are all important in determining the final morphology of the particle chains. Other models of fume formation have considered coagulation of primary nanoparticles, but have assumed that the coagulated particles are spherical; this assumption is generally invalid. Only if nucleation occurs in the very high iron vapour pressure region close to the wire electrode (such as may happen if there is unstable motion of the arc, as occurs with CO_2 shielding gas) do the nucleated particles interact while they are at sufficiently high temperature to coalesce to form spherical particles.

In our arc model, we have assumed that the oxygen-to-argon ratio is uniform throughout the arc. In reality, some demixing will occur. Results presented for an argon–oxygen arc without the presence of iron vapour indicate that demixing leads to an increase in the oxygen concentration in regions at temperatures below about 3500 K, which is the dissociation temperature of oxygen molecules [39]. Since this is the temperature range for which nucleation and particle growth occurs, demixing is expected to have an influence on the fume formation process. We plan to investigate this in future work, using a recently-developed method of applying combined diffusion coefficients to mixtures of three gases [40].

Our coupled chemical kinetic and particle formation model is zero-dimensional, which means that it neglects diffusive and convective transport of species from the surrounding gas. As was noted previously, we maintain a constant pressure in our calculations by replacing nucleated and condensed Fe atoms and FeO molecules by argon atoms. In practice, some gas-phase iron and oxygen species will be transported, together with argon, into the region in which nucleation and condensation are taking place. To treat such a process accurately requires a two- or three-dimensional model that couples the particle formation to the arc processes. The two-dimensional model of Boselli et al. [13] is the only published example of such a model applied to fume formation. Another effect that has not been considered is Brownian diffusion of the nanoparticles, which could lead to particles deviating from streamlines; this would be difficult to resolve with the computational meshes that are typically used in arc models.

A further question to be considered is the mixing of the surrounding air into the shielding gas. In the case of MIG welding, there is no oxygen in the shielding gas, but the surrounding air may reach the nucleation zone if shielding is not complete. Our results indicate that the fume particle properties in MIG welding will be very sensitive to any such mixing of air into the nucleation region. To treat such mixing would require consideration of three separate gases, argon, iron vapour and ambient air, in the model; this should be possible using the extension of combined diffusion coefficients to mixtures of three gases [40], but such a model has not yet been developed [41].

Nucleation of fume particles is predicted to occur at temperatures well below 3000 K, for which the charged-species densities are negligible under the assumption of LTE. However, there are likely to be significant deviations from LTE in the arc fringes, due mainly to diffusion of charged species under the influence of the strong gradients [42], leading to non-negligible charged-species densities. As noted above, Tashiro et al. [12] investigated the influence of particle charging on nucleation. Another effect that may be significant is ion-induced nucleation, which provides an additional nucleation mechanism [43, 44]. This has been considered by Vishnyakov et al. [16] in their calculation of fume formation in shielded metal arc welding, as was noted in the Introduction.

A complete model of fume formation in MIG/MAG welding therefore requires several additional features to be included, such as demixing of the argon–oxygen mixture, mixing of the surrounding air into the shielding gas, deviations from LTE, full coupling of particle-formation and arc processes, additional oxidation of the particles that are produced, and a calculation of the morphology of the secondary particles produced by coagulation of the primary particles. We have shown that it is important to consider the gas-phase chemical kinetics. Development of a model with all these features is a demanding task, but most of the individual components have been considered in the works discussed in this section, and the model presented in this paper.

Conclusions

We have presented predictions of fume particle nucleation and growth using a model that couples chemical kinetics, particle nucleation and particle growth by condensation. The model allows the size, composition and number density of the particles to be predicted. We have found that consideration of chemical kinetics can give significantly different gas-phase compositions from those calculated using chemical equilibrium, particularly for high quench rates and moderate to low iron vapour concentrations. However, to fully understand the effect of chemical kinetics on fume formation, further work is required to compare the influence on fume particle nucleation and growth of chemical equilibrium gas-phase compositions with compositions calculated using chemical kinetics.

As well as giving results for constant quench rates, we have also presented results calculated using parameters obtained from a three-dimensional MIG/MAG arc model.

We have shown that the presence of oxygen has a very significant influence on the size, composition and number density of fume particles formed in MIG/MAG welding. Specifically, when sufficient oxygen is present for FeO, rather than Fe, to be nucleated, the particle size is much smaller, and the number density of particles is correspondingly larger. The amount of oxygen required for FeO nucleation to be more rapid than Fe nucleation depends on the concentration of iron vapour, but is relatively small; for example an oxygen-to-argon ratio of only 0.04 mol% is required for FeO nucleation to dominate for an iron vapour mole fraction of 20%. It is possible for both FeO and Fe nucleation to occur, but for conditions typical of MAG welding (oxygen-to-argon ratios of 1% or higher, and iron vapour mole fraction of 10–20% in the regions of temperatures below 3000 K where nucleation takes place), only FeO will nucleate. The particles grow by condensation of both Fe and FeO, and the final composition depends on the relative amounts of iron vapour and oxygen present in the gas.

Calculations of particle formation and growth along streamlines in MIG and MAG arcs have confirmed the importance of oxygen in determining the particle size and number density. However, a complete model of fume formation in welding arcs requires the inclusion of many additional factors, such as full coupling of fume formation and arc processes, coagulation into chains of the primary particles formed by nucleation and condensation, and subsequent oxidation of the particles that are formed. All these factors have been considered separately in previous work, but combining them into a single model is highly challenging.

References

1. Antonini JM (2003) Health effects of welding. Crit Rev Toxicol 33(1):61–103
2. Matrat M, Guida F, Mattei F, Cenee S, Cyr D, Fevotte J, Sanchez M, Menvielle G, Radoi L, Schmaus A, Woronoff AS, Luce D, Stucker I, Icare Study G (2016) Welding, a risk factor of lung cancer: the ICARE study. Occup Environ Med 73(4):254–261
3. Cosgrove M (2015) Arc welding and airway disease. Weld World 59(1):1–7
4. Shigeta M, Murphy AB (2011) Thermal plasmas for nanofabrication. J Phys D Appl Phys 44(17):174025
5. Girshick SL, Chiu C-P, McMurry PH (1988) Modelling particle formation and growth in a plasma synthesis reactor. Plasma Chem Plasma Process 8(2):145–156
6. Girshick SL, Chiu C-P (1989) Homogeneous nucleation of particles from the vapor phase in thermal plasma synthesis. Plasma Chem Plasma Process 9(3):355–369

7. Girshick SL, Chiu C-P, Muno R, Wu CY, Yang L, Singh SK, McMurry PH (1993) Thermal plasma synthesis of ultrafine iron particles. J Aerosol Sci 24(3):367–382
8. Bilodeau J-F, Proulx P (1996) A mathematical model for ultrafine iron powder growth in a thermal plasma. Aerosol Sci Technol 24(3):175–189
9. Lei P, Boies AM, Calder S, Girshick SL (2012) Thermal plasma synthesis of superparamagnetic iron oxide nanoparticles. Plasma Chem Plasma Process 32(3):519–531
10. Deam RT, Simpson SW, Haidar J (2000) A semi-empirical model of the fume formation from gas metal arc welding. J Phys D Appl Phys 33(11):1393–1402
11. Tashiro S, Zeniya T, Yamamoto K, Tanaka M, Nakata K, Murphy AB, Yamamoto E, Yamazaki K, Suzuki K (2010) Numerical analysis of fume formation mechanism in TIG welding. Q J Jpn Weld Soc 28(4):369–375
12. Tashiro S, Murphy AB, Matsui S, Tanaka M (2013) Numerical analysis of the influence of particle charging on the fume formation process in arc welding. J Phys D Appl Phys 46(22):224007
13. Boselli M, Colombo V, Ghedini E, Gherardi M, Sanibondi P (2013) Two-dimensional time-dependent modelling of fume formation in a pulsed gas metal arc welding process. J Phys D Appl Phys 46(22):224006
14. Sanibondi P (2015) Numerical investigation of the effects of iron oxidation reactions on the fume formation mechanism in arc welding. J Phys D Appl Phys 48(34):345202
15. Tashiro S, Zeniya T, Yamamoto K, Tanaka M, Nakata K, Murphy AB, Yamamoto E, Yamazaki K, Suzuki K (2010) Numerical analysis of fume formation mechanism in arc welding. J Phys D Appl Phys 43(43):043012
16. Vishnyakov VI, Kiro SA, Ennan AA (2013) Formation of primary particles in welding fume. J Aerosol Sci 58(1):9–16
17. Vishnyakov VI, Kiro SA, Ennan AA (2014) Bimodal size distribution of primary particles in the plasma of welding fume: coalescence of nuclei. J Aerosol Sci 67(1):13–20
18. Vishnyakov VI, Kiro SA, Ennan AA (2014) Multicomponent condensation in the plasma of welding fumes. J Aerosol Sci 74(1):1–10
19. Rumminger MD, Reinelt D, Babushok V, Linteris GT (1999) Numerical study of the inhibition of premixed and diffusion flames by iron pentacarbonyl. Combust Flame 116(1–2):207–219
20. Chase MW, Jr. (ed) (1998) NIST–JANAF thermochemical tables, vol Monograph 9. J. Phys. Chem. Ref. Data, 4th edn
21. Girshick SL, Chiu C-P (1990) Kinetic nucleation theory: a new expression for the rate of homogeneous nucleation from an ideal supersaturated vapor. J Chem Phys 93(2):1273–1277
22. Friedlander SK (1983) Dynamics of aerosol formation by chemical reaction. Ann NY Acad Sci 404(1):354–364
23. Iida T, Guthrie RIL (1988) The physical properties of liquid metals. Oxford University Press, Oxford
24. Butcher JC (1964) Integration processes based on Radau quadrature formulas. Math Comput 18(86):233–244
25. Hairer H, Wanner E (1999) Stiff differential equations solved by Radau methods. J Comput Appl Math 111(1–2):93–111
26. Murphy AB (2013) Influence of metal vapour on arc temperatures in gas–metal arc welding: convection versus radiation. J Phys D Appl Phys 46(22):224004
27. Murphy AB (1993) Combined diffusion coefficients in equilibrium mixtures of dissociating gases. J Chem Phys 99(2):1340–1343
28. Murphy AB (2014) Calculation and application of combined diffusion coefficients in thermal plasmas. Sci Rep 4:4304
29. Murphy AB, Arundell CJ (1994) Transport coefficients of argon, nitrogen, oxygen, argon–nitrogen and argon–oxygen plasmas. Plasma Chem Plasma Process 14(4):451–490
30. Murphy AB (2010) The effects of metal vapour in arc welding. J Phys D Appl Phys 43(43):434001
31. Cram LE (1985) Statistical evaluation of radiative power losses from thermal plasmas due to spectral lines. J Phys D Appl Phys 18(3):401–411
32. Menart J, Malik S (2002) Net emission coefficients for argon–iron thermal plasmas. J Phys D Appl Phys 35(9):867–874
33. Gleizes A, Cressault Y, Teulet P (2010) Mixing rules for thermal plasma properties in mixtures of argon, air and metallic vapours. Plasma Sources Sci Technol 19(5):055013
34. Jonsson PG, Murphy AB, Szekely J (1995) The influence of oxygen additions on argon-shielded gas metal arc-welding processes. Weld J 74(2):48s–58s
35. Colombo V, Ghedini E, Sanibondi P (2008) Thermodynamic and transport properties in non-equilibrium argon, oxygen and nitrogen thermal plasmas. Prog Nucl Energy 50(8):921–933

36. Schnick M, Fuessel U, Hertel M, Haessler M, Spille-Kohoff A, Murphy AB (2010) Modelling of gas-metal arc welding taking into account metal vapour. J Phys D Appl Phys 43(43):434008
37. Ogino Y, Hirata Y, Murphy AB (2016) Numerical simulation of GMAW process using Ar and an Ar–CO_2 gas mixture. Weld World 60(2):345–353
38. Hertel M, Rose S, Füssel U (2016) Numerical simulation of arc and droplet transfer in pulsed GMAW of mild steel in argon. Weld World 60(5):1055–1061
39. Murphy AB (1997) Demixing in free-burning arcs. Phys Rev E 55(6):7473–7494
40. Zhang XN, Murphy AB, Li HP, Xia WD (2014) Combined diffusion coefficients for a mixture of three ionized gases. Plasma Sources Sci Technol 23(6):065044
41. Murphy AB (2015) A perspective on arc welding research: the importance of the arc, unresolved questions and future directions. Plasma Chem Plasma Process 35(3):471–489
42. Boselli M, Colombo V, Ghedini E, Gherardi M, Rotundo F, Sanibondi P (2014) Investigation of thermal nonequilibrium in a plasma arc welding process: modeling and diagnostics. IEEE Trans Plasma Sci 42(5):1237–1244
43. Girshick SL, Rao NP, Kelkar M (1996) Model for ion-induced nucleation based on properties of small ionic clusters. J Vac Sci Technol A 14(2):529–534
44. Vishnyakov VI, Kiro SA, Ennan AA (2011) Heterogeneous ion-induced nucleation in thermal dusty plasmas. J Phys D Appl Phys 44(21):215201